Journal of Alloys and Compounds 489 (2010) 535–540

Contents lists available at ScienceDirect

Journal of Alloys and Compounds

journal homepage: www.elsevier.com/locate/jallcom

Liquid phase separation and microstructure characterization in a designed Al-based amorphous matrix composite with spherical crystalline particles

Jie He*, Haiquan Li, Baijun Yang, Jiuzhou Zhao, Haifeng Zhang, Zhuangqi Hu

Institute of Metal Research, Chinese Academy of Sciences, Shenyang 110016, PR China

ARTICLE INFO

Article history:
Received 16 June 2009
Received in revised form
16 September 2009
Accepted 17 September 2009
Available online 25 September 2009

Keywords:
Amorphous materials
Metallic glasses
Composite materials
Rapid solidification
Phase transitions
Microstructure

ABSTRACT

The solidification process of the immiscible alloys exhibit a unique opportunity in designing the composites with the spherical crystalline particles dispersed in the amorphous metal matrix. The typical Al–Pb immiscible alloy and the additional elements Ni, Y and Co were selected, and the $Al_{82.87}Pb_{2.5}Ni_{4.88}Y_{7.8}Co_{1.95}$ multicomponent immiscible alloy has been designed. The ribbon samples of the multicomponent alloy were prepared by using the melt spinning technique. The ribbons were characterized by the scanning electron microscopy (SEM). The phase constitution and transformation were studied by the X-ray diffraction (XRD) and the differential scanning calorimeter (DSC). It was revealed in the as-quenched ribbons the Al-based metallic glass matrix is embedded by the spherical crystalline Pb-rich particles. The microstructure evolution, the glass formation and the thermal stability of the as-prepared composite have been discussed in detail. A method has been developed based on the mechanism of the liquid–liquid phase transformation in the miscibility gap of the multicomponent immiscible alloy to produce the spherical crystalline particles in the amorphous matrix.

1. Introduction

Immiscible systems, such as Al–Pb, Cu–Pb and Cu–Fe alloys, are characterized by the stable or metastable miscibility gap in the liquid state. When a single-phase liquid is undercooled into the gap, the liquid–liquid phase transformation takes place and the liquid separates into two liquids [1]. Many investigations on the solidification process of the immiscible alloys have been carried out by using the experimental method and numerical simulation [2–6]. The progress in the solidification control has been made to obtain the refinement microstructure. The effects of the magnetic field [7], the convective flow [8], the gravity level [9] and the droplet interaction with the solidification interface [10] on the solidification process were investigated recently. It was indicated that the microstructure evolution is strongly dependent on the thermodynamics and kinetics of the liquid phase separation in the miscibility gap. Generally, the liquid–liquid phase transformation begins with the nucleation of the liquid minority phase in form of spheres. These nucleated spheres grow by the solute diffusion in the supersaturated matrix [1,4,11]. Under the condition of the rapid solidification, the spherical particles in the micron scale are dispersed in the matrix phase after the complete solidification. Such a composite microstructure with the *in situ* crystalline spheres embedded into the crystalline alloy matrix is normally formed in various immiscible alloys [12–16]. Thus, it can be seen that the liquid immiscible systems present a unique opportunity in designing the composites with the sphere-dispersed microstructure.

To solve the problem of the low plastic strain of the monolithic metallic glass, the metallic glass matrix composites consisting of the crystalline reinforcement phases in the glassy matrix have been developed by different methods such as the nanocrystal precipitation [17–21], the addition of the crystalline particles or fibers [22–25], and the *in situ* formation of dendrites [26–30]. Especially, the two latter methods were used to prepare the metallic glass matrix composites. With the addition of the crystalline particles or fibers, the infiltration takes place at a temperature above the liquidus temperature. The choice of the *ex situ* phase materials is limited to the high-melting-temperature materials such as the carbides and the refractory metals [31,32]. The *in situ* composites are synthesized by precipitating out the dendritic phase from the melt during the rapid solidification. The liquid–solid phase transformation occurs prior to the glass transition of the matrix liquid. Sun et al. [33] reported that sufficient holding time at a temperature in the liquid/solid two-phase region of the Zr-based bulk metallic glass composites will turn the *in situ* dendritic phase into the spherical particles, and the contributions of the spherical crystalline particles to the ductility and strength of the metallic glasses is much better than that of the dendritic phase [34]. Recently, the heterogeneity microstructure was observed for some bulk metallic glass systems, which consist of a strong repulsive tendency of components. The dispersed particles were formed due to the phase separation in the bulk Cu-based [35,36], Fe-based [37,38],

* Corresponding author. Tel.: +86 24 23971905; fax: +86 24 23971918.
E-mail address: jiehe@imr.ac.cn (J. He).

0925-8388/$ – see front matter © 2009 Elsevier B.V. All rights reserved.
doi:10.1016/j.jallcom.2009.09.102

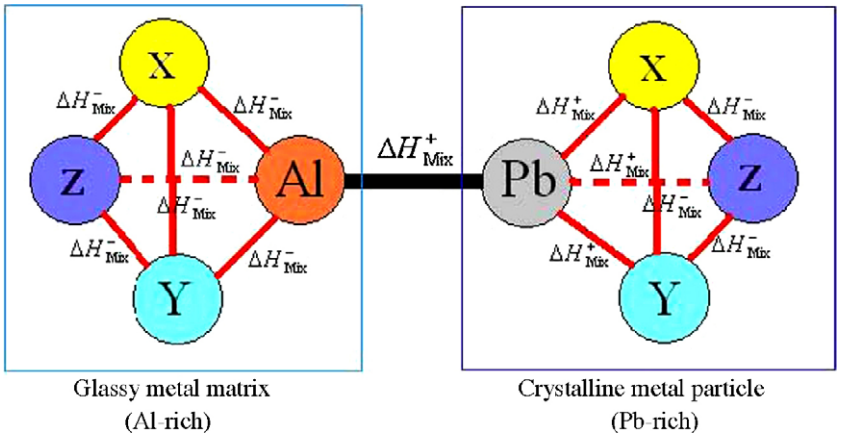

Fig. 1. Illustration of the mixing heat (ΔH_{Mix}) among the elements Al, Pb and the selected elements X, Y, Z.

Zr-based [39,40] and Ti-based [41] amorphous alloys with high glass-forming ability. However, the *in situ* formation of the spherical crystalline particles in the amorphous alloy with relative low glass-forming ability, e.g., the Al-based amorphous system was not reported so far. Little is known about the formation mechanism of the composite microstructure [37,42]. In the present work, the typical Al–Pb immiscible alloy and the additional elements Ni, Y and Co were selected. The $Al_{82.87}Pb_{2.5}Ni_{4.88}Y_{7.8}Co_{1.95}$ multicomponent immiscible alloy was designed, and the Al-based metallic glass matrix composites with the spherical crystalline Pb-rich particles have been developed. In this paper, a method has been presented based on the liquid–liquid phase transformation in the miscibility gap to produce the spherical crystalline particle in the amorphous matrix. The microstructure evolution, the glass formation and the thermal stability of the as-quenched composite have been discussed in detail.

2. Experimental procedures

The liquid-state phase separation into two liquids takes place during cooling from the single-phase liquid of Al–Pb alloy into the miscibility gap. The spherical Pb particles are distributed in the α-Al matrix after the complete solidification. The mutual solubility of the components Al and Pb in the liquid and solid states is very small. In order to obtain the Al-based amorphous matrix composites containing the spherical crystalline Pb-rich particles, the additional elements X, Y, Z should be selected and added into the Al–Pb immiscible alloy. According to Inoue's empirical rule [43], the high negative heat of mixing among the main constitution element Al and the selected elements X, Y, Z is required to ensure the Al–X–Y–Z alloy to be an amorphous system with relative high glass-forming ability. Furthermore, to make the Pb phase in form of the spherical crystalline particles be dispersed in the Al-based amorphous matrix, the positive heat of mixing between Pb and the main selected elements X, Y, Z should be required, as illustrated by Fig. 1. Ideally, the X–Pb, Y–Pb and Z–Pb alloys are immiscible systems, respectively.

According to the above analysis, in this work, the metallic elements Ni, Co, Y are selected. The mixing heats between Al and the selected elements Ni, Y, and Co are negative, while the mixing heats of Ni–Pb and Co–Pb are positive, as listed in Table 1. The Al–Ni–Y–Co system has relative high glass-forming ability [45]. According to the binary alloy phase diagram [46], the Ni–Pb and Co–Pb alloys are immiscible systems. The Al–Pb–Ni–Y–Co alloy is a multicomponent immiscible system. It is expected that due to the negative heat of mixing the selected elements Ni, Y and Co will be mainly distributed in the Al-rich matrix liquid during the liquid-state phase separation in the miscibility gap. To ensure the occurrence of the liquid–liquid phase separation during the rapid solidification, a hypermonotectic Al–2.5 at% Pb alloy was selected. Consequently, the composition of the multicomponent immiscible alloy was optimized and designed as $Al_{82.87}Pb_{2.5}Ni_{4.88}Y_{7.8}Co_{1.95}$.

Table 1
Heats of mixing in liquid binary systems [44], kJ/mol.

	Al	Pb	Ni	Y	Co
Al	0	+11	−22	−38	−19
Pb		0	+12	−48	+17
Ni			0	−31	0
Y				0	−22
Co					0

Ingots with the nominal compositions of $Al_{82.87}Pb_{2.5}Ni_{4.88}Y_{7.8}Co_{1.95}$ were prepared by arc melting the component elements with a purity of 99.9% or higher under a Ti-gettered argon atmosphere in a water-cooled copper mold. The alloys were remelted several times. The arc-melted slow-cooled ingots were cut, and the cross-section was polished and etched. Rapidly solidified ribbon samples were prepared by remelting the alloy ingots in quartz tubes, and ejecting with an overpressure of 50 kPa through a nozzle onto a Cu single roller rotating with a surface linear velocity of 40 m/s. The ribbons have a thickness of about 60 μm and a width of about 3 mm. The glass transition and crystallization temperatures were investigated in a Perkin-Elmer differential scanning calorimeter (DSC-7) under flowing purified argon. A heating rate of 0.667 K/s was employed. DSC studies of the annealed samples were accomplished up to 1473 K in an argon atmosphere using a Netzsch 404 DSC at a heating/cooling rate of 0.333 K/s. The as-prepared ribbons were annealed respectively at temperatures 550, 600 and 700 K. The X-ray diffraction (XRD) experiments were performed for the as-prepared and as-annealed ribbons by using monochromatic Cu Kα radiation for a 2θ range of 20–80°. The scanning electron microscopy (SEM) and transmission electron microscopy (TEM) linked with an energy dispersive X-ray spectroscopy (EDX) were employed to analyze the microstructure and phase composition of the composites. The average size, the size distribution and the volume fraction of the spherical particles were determined by using SISCIAS image analysis system.

3. Results and discussion

3.1. Solidification microstructure

The solidification microstructure of the cross-section of the arc-melted and slow-cooled $Al_{82.87}Pb_{2.5}Ni_{4.88}Y_{7.8}Co_{1.95}$ alloy ingot is presented in Fig. 2. It shows the phases are distinguished by dark, gray and white color. The EDX analysis indicates that the white spherical particles are Pb-rich phase, and a composition of $Al_{8.5}Pb_{86.4}Ni_{1.7}Y_{2.3}Co_{1.1}$ is measured. Lower Al, Ni, Y and Co concentrations are detected in the particles compared with the gross composition of the ingot. In the gray lamellar phase no Pb is detected. The large grey lamellas have a composition of $Al_{67.49}Ni_{13}Y_{14.53}Co_{4.98}$. The dark phase between the large grey lamellas turns out to be essentially a two-phase structure: a real dark phase with embedded small grey lamellas, as shown in the inset of Fig. 2. The EDX analysis shows the small gray phases are enriched with Al, Ni, and Co, while a composition of $Al_{92.53}Ni_{1.09}Y_{5.9}Co_{0.49}$ is measured for the dark areas. It indicates that the element Pb is almost distributed in the white particles. The solid solubility of Pb in the dark and gray areas is neglectable.

Fig. 3 indicates the back-scattered electron micrograph of the cross-section of the as-prepared ribbon sample. It shows a heterogeneous microstructure spread over the whole sample. The white spherical particles are homogeneously distributed in the gray matrix. Locally, an average composition of $Al_{69.52}Pb_{16.43}Ni_{3.91}Y_{8.62}Co_{1.52}$ is measured for the white spheres,

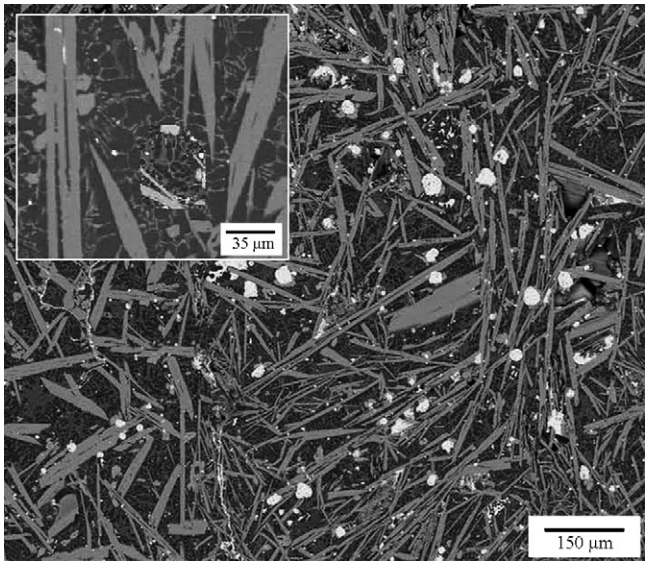

Fig. 2. SEM backscattered electron images of the cross-section of the arc-melted and slow-cooled alloy ingot.

and an average $Al_{83.39}Pb_{1.15}Ni_{5.26}Y_{7.58}Co_{2.33}$ is detected for the gray areas of the SEM image, respectively. The composition of the spherical particles strongly deviates from the nominal composition. The spherical particles are depleted in Al, and mainly enriched in Pb. The image analysis shows that the volume fraction of the white spheres is about 12%. The average diameter of the spheres is about 0.6 μm near the free side (FS), and 50 nm near the wheel side (WS) of the ribbon.

3.2. Phase constitution and transformation

The phase structure of the slow-cooled $Al_{82.87}Pb_{2.5}Ni_{4.88}Y_{7.8}Co_{1.95}$ alloy ingot and as-prepared ribbon sample has been analyzed by the X-ray diffraction experiments, and the results are shown in Fig. 4. The slow-cooled alloy ingot is mainly composed of Al, Pb, Al_3Y, Al_9Co_2, and Al_3Ni. It can be confirmed that the white spherical particles in Fig. 2 are Pb phase. Compared with that of the slow-cooled alloy ingot, the X-ray

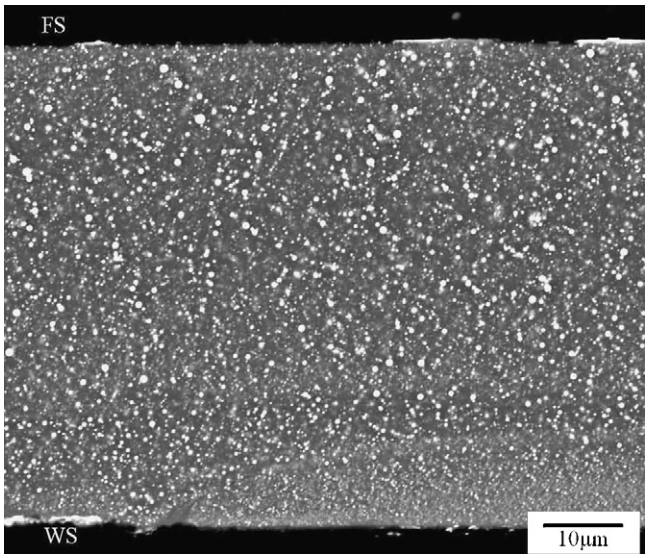

Fig. 3. SEM backscattered electron images of the cross-section of the as-prepared ribbon sample.

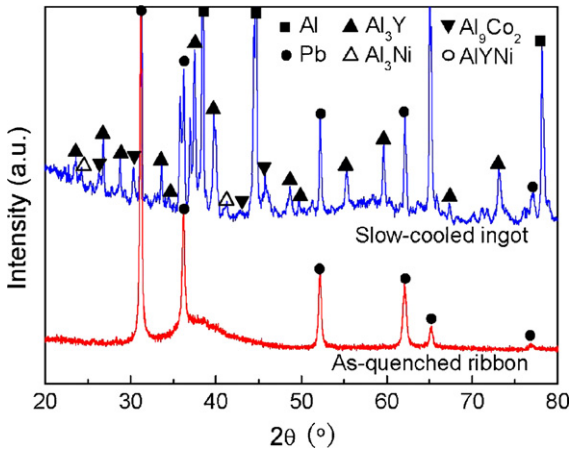

Fig. 4. XRD patterns of the slow-cooled alloy ingot and the as-prepared ribbon sample.

diffraction patterns of the as-prepared ribbon sample indicate, except for the sharp peaks of Pb, the sharp peaks of Al, Al_3Y, Al_9Co_2 and Al_3Ni phases have disappeared. The sharp peaks of Pb superimpose on a broad scattering hump characteristic of an amorphous phase. The diffraction peaks with maxima at $2\theta = 31.2°$, 36.16°, 52.2°, 62.08°, 65.2°, and 77° are identified as the white spherical Pb-rich particles in Fig. 3 with face-centered cubic structure and a lattice parameter $a = 0.4914$ nm. The matrix phase is confirmed to be the amorphous phase.

A heating rate of 0.333 K/s was employed and the ribbon samples were annealed at 550, 600 and 700 K, respectively. In order to get rid of the effect of the surface crystallization, the surface layer of the annealed samples was removed by polishing before the X-ray diffraction experiments. Fig. 5 shows the X-ray diffraction patterns of the as-annealed ribbon samples at different temperatures. Compared with that of the as-quenched ribbons in Fig. 4, the XRD patterns of the ribbons annealed at 550 K indicates the existence of the weak peaks of Al except for the sharp peaks of Pb, as shown in Fig. 5. It suggests that the crystal Al has precipitated from the Al-based amorphous matrix phase [47–50]. The XRD analysis shows the nanocrystal α-Al is with face-centered cubic structure and a lattice parameter $a = 0.4049$ nm. The crystallization of the α-Al phase may primarily occur at the interface between the crystalline Pb-rich particle and the Al-based amorphous matrix. When the annealing temperature is 600 K, the Bragg peaks corresponding to the α-Al phase become more intense and narrower, indicating a slight grain coarsening. The intermetallic compounds such as Al_3Y,

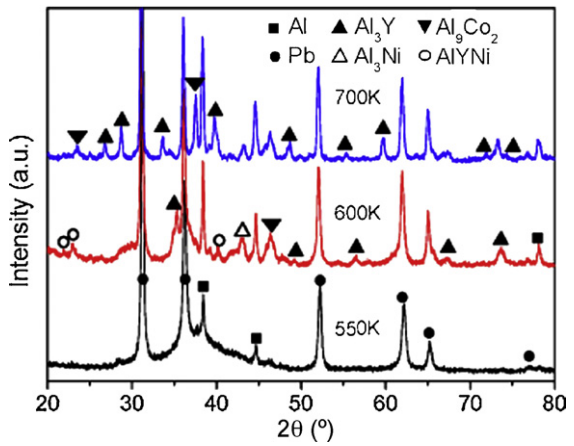

Fig. 5. XRD patterns of ribbon sample annealed at different temperatures.

Al_3Ni, AlYNi, and Al_9Co_2 have been formed during this crystallization process. The X-ray diffraction patterns of the as-annealed ribbons at 700 K indicate the microstructure consists of the face-centered cubic Pb, the face-centered cubic α-Al, the rhombohedral Al_3Y, the monoclinic Al_9Co_2 and the orthorhombic Al_3Ni.

3.3. Thermal stability and glass formation

Fig. 6 shows the DSC curves of the as-prepared ribbon samples using a heating rate of 0.667 K/s. The $Al_{85.37}Ni_{4.88}Y_{7.8}Co_{1.95}$ alloy ribbons without element Pb were also prepared by the melt spinning technique. From the DSC curve of $Al_{85.37}Ni_{4.88}Y_{7.8}Co_{1.95}$ alloy ribbons, the glass transition temperature, T_g, and onset temperature of crystallization, T_x, are about 530 and 555 K, respectively, as indicated in Fig. 6(a). There exist three sharp peaks of exothermic heat reaction due to the crystallization after the endothermic heat event of the glass transition. The DSC trace of the composite ribbons reveals that the glass transition and onset crystallization temperatures are about 517 and 540 K, respectively, as shown in the inset in Fig. 6. Only one sharp peak of the exothermic heat reaction due to the crystallization is observed in Fig. 6(b). The total enthalpy of the crystallization decreases from 164 J/g for the Al-based monolithic metallic glass to 110.5 J/g for the Al-based metallic glass matrix composites. The glass transition and onset crystallization temperatures of the $Al_{82.87}Pb_{2.5}Ni_{4.88}Y_{7.8}Co_{1.95}$ composite strongly deviate from that of the $Al_{85.37}Ni_{4.88}Y_{7.8}Co_{1.95}$ monolithic metallic glass. This indicates that the element Pb has the significant effects on the glass transition temperature as well as the crystallization transformation process of the glassy phase. The element Pb promotes the formation of the crystalline phase in the $Al_{82.87}Pb_{2.5}Ni_{4.88}Y_{7.8}Co_{1.95}$ metallic glass matrix composites.

However, it is worthy to note that the glass transition and onset crystallization temperatures of the $Al_{82.87}Pb_{2.5}Ni_{4.88}Y_{7.8}Co_{1.95}$ composite are approximately 14 K lower than that of the $Al_{85.37}Ni_{4.88}Y_{7.8}Co_{1.95}$ monolithic amorphous alloy, respectively. The $Al_{82.87}Pb_{2.5}Ni_{4.88}Y_{7.8}Co_{1.95}$ composite and the $Al_{85.37}Ni_{4.88}Y_{7.8}Co_{1.95}$ amorphous alloy exhibit a similar supercooled temperature region ($\Delta T_x \approx 14$ K). The lower onset crystallization temperature corresponds to a lower thermal stability of the glassy matrix against crystallization. This can be attributed to the alloy composition and the spherical crystalline Pb-rich particles in the composites that may act as the crystallization nucleation site to induce heterogeneous nucleation. Considering that the element Pb also leads to a decrease in the final melting temperature, T_l, of the $Al_{82.87}Pb_{2.5}Ni_{4.88}Y_{7.8}Co_{1.95}$ composites, the reduced glass transition temperature, $T_{rg} = T_g/T_l$, may have a very little change in comparison with that of the $Al_{85.37}Ni_{4.88}Y_{7.8}Co_{1.95}$ amorphous alloys.

3.4. Microstructure formation

Fig. 7 shows the DSC heating/cooling traces of the $Al_{82.87}Pb_{2.5}Ni_{4.88}Y_{7.8}Co_{1.95}$ alloy. The heating trace is characterized by the typical sharp endothermic peak due to eutectic melting at $T_e = 902$ K and the extended tail of final melting at $T_l = 1204$ K. The DSC cooling trace indicates that the first deviation from the baseline at a demixing temperature is due to the liquid–liquid phase separation. The $Al_{82.87}Pb_{2.5}Ni_{4.88}Y_{7.8}Co_{1.95}$ multicomponent monotectic alloy is characterized by an onset temperature for the liquid phase separation, $T_{sep} \approx 1359$ K, and a monotectic temperature, $T_{mono} \approx 1134$ K. The dome height of the miscibility gap, ΔT, defined as $T_{sep} - T_{mono}$, is determined to be 225 K. The liquid–liquid phase transformation in the miscibility gap can occur by two mechanisms, i.e., by the liquid-state nucleation and growth or by the liquid-state spinodal decomposition [51]. Due to a smaller degree of local undercooling, the liquid–liquid phase transformation takes place by liquid-state nucleation and growth mechanism rather than by liquid-state spinodal decomposition [1].

The microstructure formation of the present metallic glass matrix composites strongly depends on the kinetics of the liquid-state nucleation and growth. Because the Al–Pb, Ni–Pb and Co–Pb alloys are immiscible systems with the positive heat of mixing, there exists the repulsive interaction between Pb atom and Al, Ni, Co atoms. The solubility of Pb in the single-phase liquid is limited. When the liquid is undercooled into the miscibility gap, the supersaturation of Pb gradually increases with the temperature falling. The driving force for the nucleation of the Pb-rich spheres increases with decreasing temperature. Once the liquid phase separation begins with the nucleation of the Pb-rich phase in form of the liquid sphere, the nucleation rate will increase sharply. The solubility of Pb in the single-phase liquid decreases continuously, and the supersaturation gradually decreases from a peak value [52]. The nucleated spheres grow by the solute diffusion. During the growth and coagulation of the Pb-rich spheres, the concentration and supersaturation of Pb in the liquid Al-rich matrix decrease continuously. As a result, the liquid matrix mainly consists of Al, Ni, Co, and Y. As is known, the equilibrium solidification temperature of the bulk Pb is about 600.6 K, which is higher than the glass transition

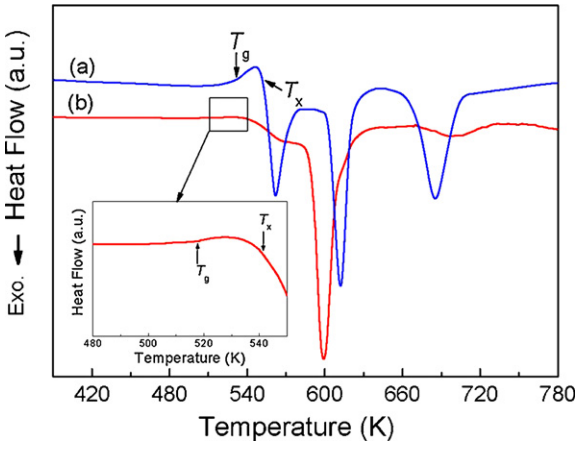

Fig. 6. DSC curves of the as-prepared ribbon samples using a heating rate of 0.667 K/s: (a) $Al_{82.87}Pb_{2.5}Ni_{4.88}Y_{7.8}Co_{1.95}$ alloy ribbon sample, (b) $Al_{85.37}Ni_{4.88}Y_{7.8}Co_{1.95}$ alloy ribbon sample.

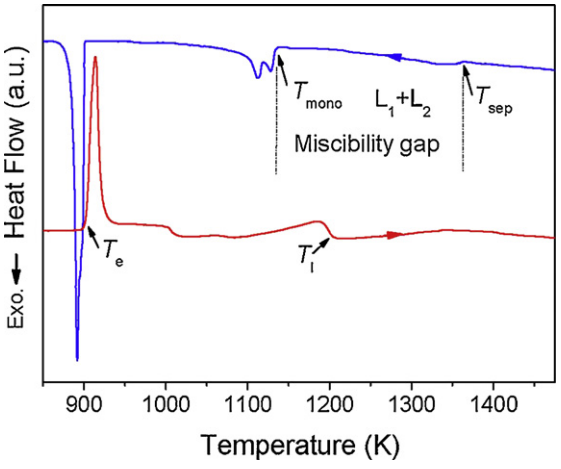

Fig. 7. DSC curves of the annealed $Al_{82.87}Pb_{2.5}Ni_{4.88}Y_{7.8}Co_{1.95}$ alloy ribbon samples upon heating and cooling at a heating/cooling rate of 0.333 K/s. L_1 and L_2 denote Al-rich and Pb-rich liquids, respectively.

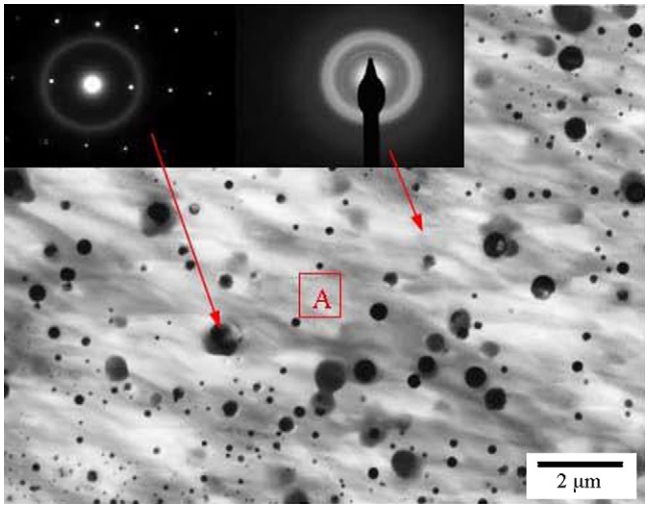

Fig. 8. TEM image of the composite showing the presence of the spherical crystalline Pb-rich particles in the amorphous matrix. SADP recorded from one of the Pb-rich particles taken along the [$\bar{1}$ 1 2] zone axis and the matrix.

temperature 517 K of the liquid matrix. However, the undercooling of the metal droplet has a correlation with the droplet size [53]. For instance, the undercooling degrees of emulsified Sn droplets in diameter of 275 and 2 μm reach 55 and 175 K, respectively [54]. Under the condition of the nonequilibrium solidification, the glass transition of the liquid Al-rich matrix may occur prior to the freezing of the liquid Pb-rich spheres. The liquid matrix with relative high glass-forming ability transits into the glassy phase by the rapid solidification. It is further confirmed by the corresponding selected area diffraction pattern (SADP), as shown in the right inset in Fig. 8. The liquid Pb-rich spheres produced by the liquid phase separation subsequently solidify into the crystalline particles at a lower temperature. Fig. 9 shows the magnified image of the matrix region 'A' in Fig. 8. It reveals that there exist smaller crystalline Pb-rich particles in the Al-based glassy matrix. The size distributions of the big Pb-rich particles (as shown in Fig. 8) and the small ones (as shown in Fig. 9) were determined by using the image analysis system, respectively. The measured results, as indicated in Fig. 10, display two particle size populations: the big one is 0.1–1.6 μm, and the small one is 3–15 nm.

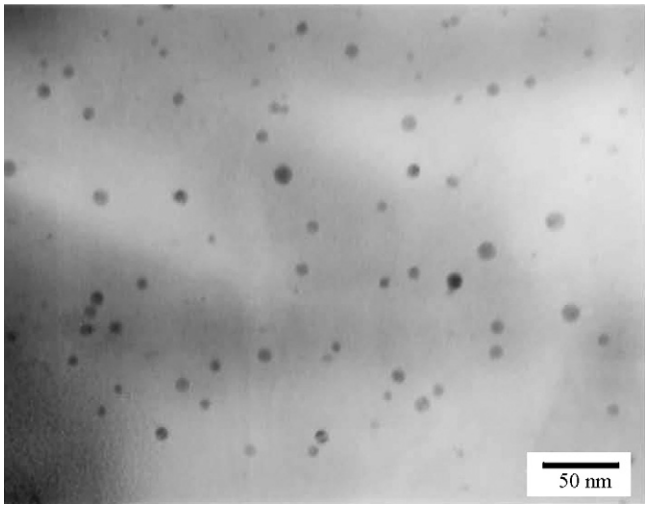

Fig. 9. TEM image of the magnified region "A" in Fig. 8.

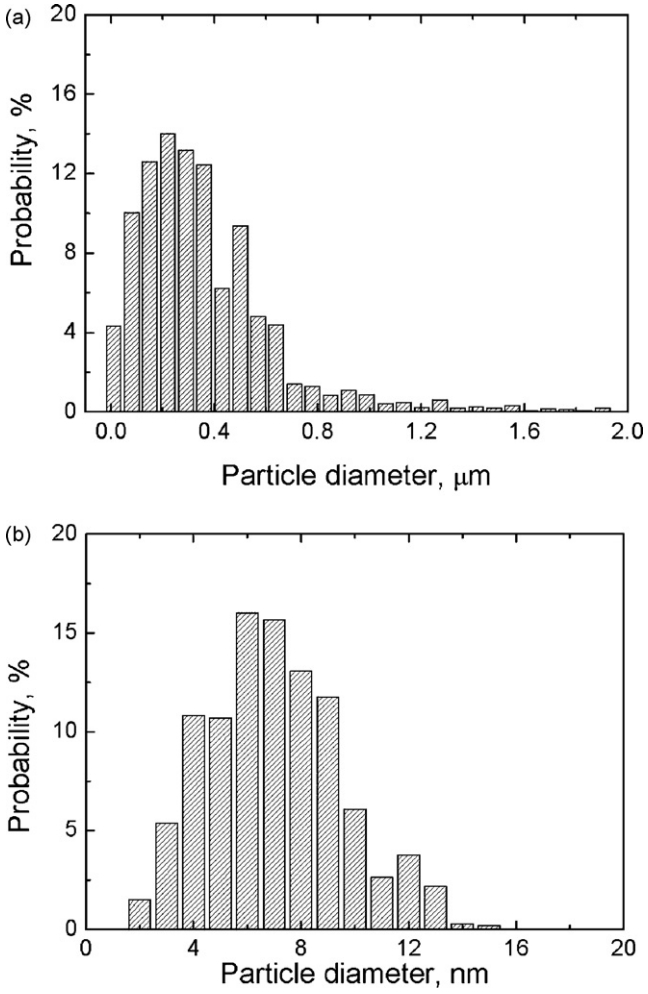

Fig. 10. Particle size distributions of (a) the primarily produced large Pb-rich particles and (b) the secondly nucleated small Pb-rich ones.

4. Conclusions

The $Al_{82.87}Pb_{2.5}Ni_{4.88}Y_{7.8}Co_{1.95}$ multicomponent immiscible system has been designed to prepare the Al-based metallic glass matrix composites containing the spherical crystalline Pb-rich particles by the rapid solidification. The single-phase alloy melt separates into the Al-rich and Pb-rich liquids during it cooling through the miscibility gap. Under the condition of the rapid solidification, the separated Al-rich and Pb-rich liquids subsequently solidify into the Al-based amorphous matrix and the spherical crystalline Pb-rich particles, respectively. The diameter of the Pb-rich particles mainly distributes in two particle size populations of 0.1–1.6 μm and 3–15 nm. The volume fraction of the Pb-rich particles is about 12%. A method has been developed based on the liquid–liquid phase separation in the miscibility gap to produce the spherical crystalline particles in the amorphous matrix. Compared with that of the $Al_{85.37}Ni_{4.88}Y_{7.8}Co_{1.95}$ monolithic metallic glass, the glass transition and onset crystallization temperatures of the $Al_{82.87}Pb_{2.5}Ni_{4.88}Y_{7.8}Co_{1.95}$ amorphous matrix composites decrease by about 14 K, and the supercooled temperature region value of the Al-based glassy matrix composites does not change significantly, but the thermal stability of the composites lowers.

Acknowledgements

This work was supported by Knowledge Innovation Program of Chinese Academy of Sciences, National Natural Science Foundation of China (nos. 50704032 and U0837601), and Liaoning Province Natural Science Foundation of China (no. 20081009).

References

[1] L. Ratke, S. Diefenbach, Mater. Sci. Eng. R 15 (1995) 263–347.
[2] Y.J. Liu, D. Liang, J. Alloys Compd. 403 (2005) 110–117.
[3] D. Mirkovic, J. Grobner, R. Schmid-Fetzer, Acta Mater. 56 (2008) 5214–5222.
[4] M. Tomellini, J. Mater. Sci. 43 (2008) 7102–7114.
[5] Y.Z. Chen, F. Liu, G.C. Yang, X.Q. Xu, Y.H. Zhou, J. Alloys Compd. 427 (2007) L1–L5.
[6] B.C. Luo, H.P. Wang, B.B. Wei, Chin. Sci. Bull. 54 (2009) 183–188.
[7] J. Wang, Y.B. Zhong, W.L. Ren, Z.S. Lei, Z.M. Ren, K.D. Xu, Acta Phys. Sin. 58 (2009) 893–900.
[8] H.L. Li, J.Z. Zhao, Q.X. Zhang, J. He, Metall. Mater. Trans. A 39 (2008) 3308–3316.
[9] A.P. Silva, J.E. Spinelli, A. Garcia, J. Alloys Compd. 480 (2009) 485–493.
[10] P.L. Schaffer, R.H. Mathiesen, L. Arnberg, Acta Mater. 57 (2009) 2887–2895.
[11] J. He, J.Z. Zhao, L. Ratke, Acta Mater. 54 (2006) 1749–1757.
[12] A.C. Sandlin, J.B. Andrews, P.A. Curreri, Metall. Trans. A 19 (1988) 2665–2669.
[13] H. Yasuda, I. Ohnaka, O. Kawakami, K. Ueno, K. Kishio, ISIJ Int. 43 (2003) 942–949.
[14] M. Kolbe, J. Brillo, I. Egry, D.M. Herlach, L. Ratke, D. Chatain, N. Tinet, C. Antion, L. Battezzati, S. Curiotto, E. Johnson, N. Pryds, Microgravity Sci. Technol. 18 (2006) 174–177.
[15] J. He, J.Z. Zhao, H.L. Li, X.F. Zhang, Q.X. Zhang, Metall. Mater. Trans. A 39 (2008) 1174–1182.
[16] A.P. Silva, J.E. Spinelli, A. Garcia, J. Alloys Compd. 475 (2009) 347–351.
[17] A.P. Tsai, N. Chandrasekhar, K. Chattopadhyay, Appl. Phys. Lett. 75 (1999) 1527–1528.
[18] A. Inoue, B.L. Shen, H. Koshibo, H. Kato, A.R. Yavari, Nat. Mater. 2 (2003) 661–663.
[19] F. Prima, M. Tomut, I. Stone, B. Cantor, D. Janickonic, G. Vlasak, P. Svec, Mater. Sci. Eng. A 375 (2004) 772–775.
[20] Q.S. Zhang, W. Zhang, G.Q. Xie, K.S. Nakayama, H. Kimura, A. Inoue, J. Alloys Compd. 431 (2007) 236–240.
[21] G. Wilde, B. Peter, H. Rosner, J. Weissmuller, J. Alloys Compd. 434–435 (2007) 286–289.
[22] H. Kato, A. Inoue, Mater. Trans. JIM 38 (1997) 793–800.
[23] R.D. Conner, R.B. Dandliker, W.L. Johnson, Acta Mater. 46 (1998) 6089–6102.
[24] H. Choi-Yim, R.D. Conner, F. Szuecs, W.L. Johnson, Acta Mater. 50 (2002) 2737–2745.
[25] D.G. Pan, H.F. Zhang, A.M. Wang, Z.Q. Hu, Appl. Phys. Lett. 89 (2006), 261904.
[26] C.C. Hays, C.P. Kim, W.L. Johnson, Phys. Rev. Lett. 84 (2000) 2901–2904.
[27] G.Y. Wang, P.K. Liaw, A. Peter, M. Freels, W.H. Peter, R.A. Buchanan, C.R. Brooks, Intermetallics 14 (2006) 1091–1097.
[28] J. Kong, Z.T. Ye, F. Lv, J. Alloys Compd. 478 (2009) 202–205.
[29] J. Das, F. Ettingshausen, J. Eckert, Scr. Mater. 58 (2008) 631–634.
[30] J.W. Qiao, Y. Zhang, Z.L. Zheng, J.P. He, B.C. Wei, J. Alloys Compd. 477 (2009) 436–439.
[31] W. Zhang, S. Ishihara, A. Inoue, Mater. Trans. JIM 43 (2002) 1767–1770.
[32] M.H. Lee, D.J. Sordelet, J. Mater. Res. 21 (2006) 492–499.
[33] G.Y. Sun, G. Chen, C.T. Liu, G.L. Chen, Scr. Mater. 55 (2006) 375–378.
[34] G.Y. Sun, G. Chen, G.L. Chen, Intermetallics 15 (2007) 632–634.
[35] J.C. Oh, T. Ohkubo, Y.C. Kim, E. Fleury, K. Hono, Scr. Mater. 53 (2005) 165–169.
[36] K.B. Kim, J. Das, F. Baier, M.B. Tang, W.H. Wang, J. Eckert, Appl. Phys. Lett. 88 (2006), 051911.
[37] T. Nagase, A. Yokoyama, Y. Umakoshi, Mater. Trans. JIM 47 (2006) 1105–1114.
[38] K. Ziewiec, Z. Kedzierski, J. Alloys Compd. 480 (2009) 306–310.
[39] M.U. Kim, J.P. Ahn, H.K. Seok, E. Fleury, H.J. Chang, D.H. Kim, P.R. Cha, Y.C. Kim, Met. Mater. Int. 15 (2009) 193–196.
[40] X.H. Du, J.C. Huang, H.M. Chen, H.S. Chou, Y.H. Lai, K.C. Hsieh, J.S.C. Jang, P.K. Liaw, Intermetallics 17 (2009) 607–613.
[41] K. Ziewiec, Z. Kedzierski, A. Zielinksa-Lipiec, J. Stepinski, S. Kac, J. Alloys Compd. 482 (2009) 114–117.
[42] J. He, H.Q. Li, J.Z. Zhao, C.L. Dai, Appl. Phys. Lett. 93 (2008), 131907.
[43] A. Inoue, Acta Mater. 48 (2000) 279–306.
[44] F.R. Boer, R. Boom, W.C.M. Mattens, A.R. Miedema, A.K. Niessen, Cohesion and Structure, 1st ed., Elsevier Science, Amsterdam, 1988.
[45] A. Inoue, N. Matsumoto, T. Masumoto, Mater. Trans. JIM 31 (1990) 493–500.
[46] H. Okamoto, Desk Handbook Phase Diagrams For Binary Alloys, 1st ed., ASM International, New York, 2000.
[47] J.Q. Wang, H.W. Zhang, X.J. Gu, K. Lu, Appl. Phys. Lett. 80 (2002) 3319–3321.
[48] Y.B. Wang, H.W. Yang, B.B. Sun, B. Wu, J.Q. Wang, M.L. Sui, E. Ma, Scr. Mater. 55 (2006) 469–472.
[49] S. Scudino, K.B. Surreddi, S. Sager, M. Sakaliyska, J.S. Kim, W. Loser, J. Eckert, J. Mater. Sci. 43 (2008) 4518–4526.
[50] K.G. Prashanth, S. Scudino, B.S. Murty, J. Eckert, J. Alloys Compd. 477 (2009) 171–177.
[51] C.W. Yuen, K.L. Lee, H.W. Kui, J. Mater. Res. 12 (1997) 314–317.
[52] J.Z. Zhao, J. He, Z.Q. Hu, L. Ratke, Z. Metallkd. 95 (2004) 362–368.
[53] J.H. Perepezko, J.L. Sebright, P.G. Hockel, G. Wilde, Mater. Sci. Eng. A 326 (2002) 144–153.
[54] J.H. Perepezko, M.J. Uttormark, Metall. Mater. Trans. A 27 (1996) 533–547.